UCRL-ID-135689

An Adaptive Optic for Correcting Low-Order Wavefront Aberrations

J. Wilhelmsen, C. Thompson

September 2, 1999

U.S. Department of Energy

Lawrence
Livermore
National
Laboratory

Work performed under the auspices of the U. S. Department of Energy by the University of California Lawrence Livermore National Laboratory under Contract W-7405-Eng-48.

This report has been reproduced
directly from the best available copy.

Available to DOE and DOE contractors from the
Office of Scientific and Technical Information
P.O. Box 62, Oak Ridge, TN 37831
Prices available from (423) 576-8401
http://apollo.osti.gov/bridge/

Available to the public from the
National Technical Information Service
U.S. Department of Commerce
5285 Port Royal Rd.,
Springfield, VA 22161
http://www.ntis.gov/

OR

Lawrence Livermore National Laboratory
Technical Information Department's Digital Library
http://www.llnl.gov/tid/Library.html

Abstract:

Adaptive Optics used for correcting low-order wavefront aberrations were tested and compared using interferometry, beam propagation, and a far-field test. Results confirm that the design and manufacturing specifications were met. Expermental data also confirms theoretical performance expectations, indicating the usefulness of these optics (especially in a laser-beam processing system), and identifying the resulting differences between the two fabrication methods used to make the optics.

Table of Contents

List of Figures

Introduction:

In this project we characterized two adaptive optics used for correcting low-order wavefront aberrations. In his book *Principles of Adaptive Optics*, Robert Tyson gives a simple definition, Adaptive optics is “a method of automatically keeping the light focused when it gets out of focus”[1]. An adaptive optic system can be as natural as the human eye, or as technological as the laser guide star system used in astronomy. When it is recognized that a laser is a light source, the simple definition above can encompass even high-power laser systems. Adaptive optics are needed in all of these systems because optical systems are not ideal; aberrations do exist. Aberrations can reduce system efficiency, or prevent a system from fulfilling its design requirements. Deformable mirrors are a widely known example of an adaptive optic.

The adaptive optics used in this project address the correction of primarily astigmatism. Other types of aberrations could include: spherical, coma, chromatic, and distortion. In an astigmatic wavefront two focal planes appear, orthogonal to one another, at different longitudinal points.

Each adaptive optic in this project is comprised of two elements. Both elements are shaped with a cubic curve such that the two elements are complimentary. Intuitively we see that in this position (neutral) the optic is like a plano piece of glass. A collimated wavefront passing through it would not be affected. When the elements are translated their profiles no longer cancel each other. The result is a quadratic phase variation deriving from the difference of the profiles. The curve used on these optics produced an astigmatic wavefront. Simply put, sliding the elements along x-axis produces astigmatism in the x-axis, and likewise sliding the elements on the y-axis produces astigmatism in the y-axis (Figure 1). The correct curve for this kind of system was developed by Luis Alvarez [2][3][4].

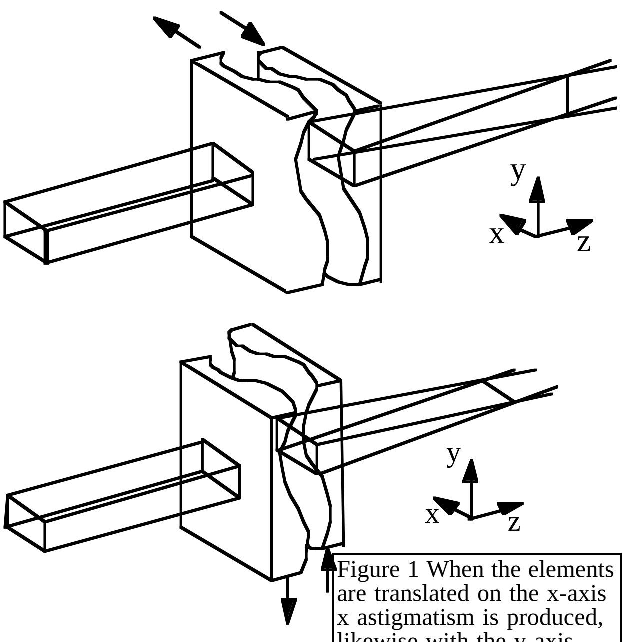

Figure 1 When the elements are translated on the x-axis x astigmatism is produced, likewise with the y-axis.

There are different kinds of adaptive optics, each with advantages and disadvantages. A feature of this optic that is both an advantage and a disadvantage is its simplicity. This optic is primarily for correcting astigmatism, other optics such as deformable mirrors can correct higher-order aberrations. The computing power required to run an adaptive optic is directly related to how complex the optic is. It follows that the optic discussed here requires less computing power than many more complicated systems. Another advantage of this more simplistic system is its continuity. A deformable mirror, while able to correct more aberrations can only do so discreetly based on the number of actuators used [5]. The disadvantage is the optics lack of ability to correct other aberrations.

An issue that optics must accommodate in high-power laser systems is the effects of thermal energy in the optical transport system. Excess thermal energy can cause the optics of a system to produce more aberrations, which are primarily astigmatic in nature. If this energy cannot dissipate before the system is used again, the resulting aberrations must be corrected using adaptive optics. The adaptive optic presented in this paper can be used to correct large, low-order aberrations leaving smaller higher-order aberrations for more sophisticated optics, like deformable mirrors. In some thermal situations the corrections necessary would be too large for a deformable mirror to correct alone.

Materials and Methodology:

Design specifications

Each optic is composed of two elements, each of which has a cubic profile determined by the following cubic equation:

$$Z=a\cdot x^3-b\cdot x-c\cdot y^3+d\cdot y$$

Where the coefficients are determined to be:

Plate 1
$a=1.63399\cdot 10^{-7}mm^{-2}$
$b=2.5931\cdot 10^{-4}$
$c=4.08497\cdot 10^{-8}mm^{-2}$
$d=1.3346\cdot 10^{-4}$

Plate 2
$a=1.63399\cdot 10^{-7}mm^{-2}$
$b=2.5931\cdot 10^{-4}$
$c=-4.08497\cdot 10^{-8}mm^{-2}$
$d=-1.3346\cdot 10^{-4}$

Once manufactured plate #2 is rotated 180°about the y-axis so that the profiles of the two lens will face each other. The a and c coefficients were chosen such that 10 mm of shift on each plate (in opposite directions) results in a wavefront Optical Path Difference (OPD) of 3λ, where λ is the operating wavelength of 600 nm with beam size of 40x80 mm. The resulting OPD is :

$$\text{OPD} = 6\cdot(n-1)\cdot(a\cdot x^2\cdot\xi + c\cdot y^2\cdot\eta),$$

where n is the index of refraction of the plate and ξ and η are the plate displacements. Note the independence of OPD on the b and d coefficients. These coefficients were chosen to minimize the amount of material that needed to be removed from the substrate during fabrication of the optic.

This optic was designed for a beam size of 40 mm by 80 mm, with a total translation of ±25 mm, resulting in the following lens apertures:
Used aperture area: 90 mm by 130 mm
Area figured: 92 mm by 132 mm
Edge aperture: 100 mm by 140 mm
These values indicate that while only 90 mm by 130 mm of the optic will actually be used when the elements are fully translated 92 mm by 132 mm will have the profile figured on them.

Fabrication

Due to the non-rotational symmetric profile required in these adaptive optics non-traditional optical fabrication techniques were explored. Two fabrication methods were attempted. Raytheon Optical Systems Inc. used small tool polishing and the Laser Science and Technology group at Lawrence Livermore National Laboratory used photolithography.

Small-Tool Polishing

With this method of fabrication a lens with a continuous curve is produced. The fabrication begins with an optical glass that has been polished flat. A small rotating tool passes over the optic grinding out the desired surface profile. One of the challenges in fabricating these optics was the combination of their size (nearly 6” on a side) and the steep incline of the curve required at the edges. The steep curvature of the optical surface was too great to measure accurately with a conventional interferometer, and the size of the optics prevented several other methods including a commonly used null corrector. Raytheon proposed an alternative method that tested the optics in transmission by immersing them in a near-index matching solution. This allowed a large surface departure to appear smaller to the measuring interferometer, making the metrology possible. A computer took this metrology information and subtracted the equation of the curve to determine how long the polishing tool would have to be kept at each location on the optic to achieve the desired curve on the next polishing cycle. Great care and several polishing runs had to be used to achieve a curve as smooth as desired by the designers. Any curve deviations, such as tooling marks, will introduce higher-order beam aberrations, or diffraction.

Photolithography

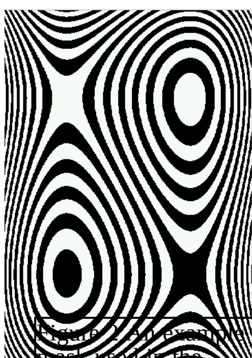

Figure 2 An example of a mask used in the photolithography of the adaptive optic. [6]

The photolithography method used by Laser Science and Technology produced 16-level phase-plate optics. In these optics the cubic curve required by the design is not continuous. Instead it is made up of different levels, created using standard multi-level photolithography techniques used in fabricating binary diffractive optics. The first step in the process is to break the profile into discreet phase levels corresponding to 1λ path difference, where λ is the design wavelength (600 nm in this case).Four masks are fabricated to create this profile on the optic. The first step in the manufacturing process is to apply a photoresist to the substrate. Then the first mask from the previous process (Figure 2) is placed on top of the coated substrate and the optic is exposed to UV illumination (Figure 3) After the pattern has been exposed onto the photoresist and the photoresist has been chemically developed the part is ready to be chemically etched. The etch rate of fused silica can be controlled so that the silica is removed at a constant pre-determined rate. The photoresist prevents the substrate from being etched as deeply as the areas where the photoresist has been developed. To achieve a multi-level phase plate, this process must be repeated. The equation for determining the number of masks required for an N level phase plate is 2^n=N,

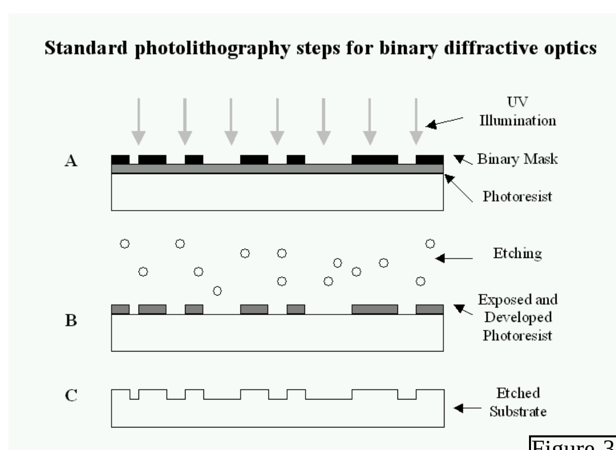

Figure 3 [6]

where n is the number of masks. It follows that 4 masks are required for each 16 level phase plate for a total of 8 masks for the optic [7]. During fabrication each successive mask must be aligned nearly perfectly to the previous etch. Misalignment results in increased diffraction. When the optic is completed the Anti-Reflection (AR) coating could be applied. The optic as tested, did not have an AR coating.

Tests

Three tests were run to characterize these optics: Interferometry, Beam Propagation and Far Field. The data collected for all of these tests can be returned as images. In the interferometry test, peak to valley (PV), RMS, and sagitta (sag) numerical values were also tabulated. The set-up for each test is slightly different, but the positioning of the adaptive optic is constant for all three. The set-up for the Raytheon optic has the opposite y-axis as the set-up for the Phase-plate because the position of the stepper motor was switched.

Interferometry

This test is used to analyze the wavefront after the beam passes through the optic. From the measurements we expect to see astigmatic wavefronts caused by the translation of the optical elements. Interferometric data should confirm this along with showing the higher-order residual error due to fabrication. A Wyko 6000

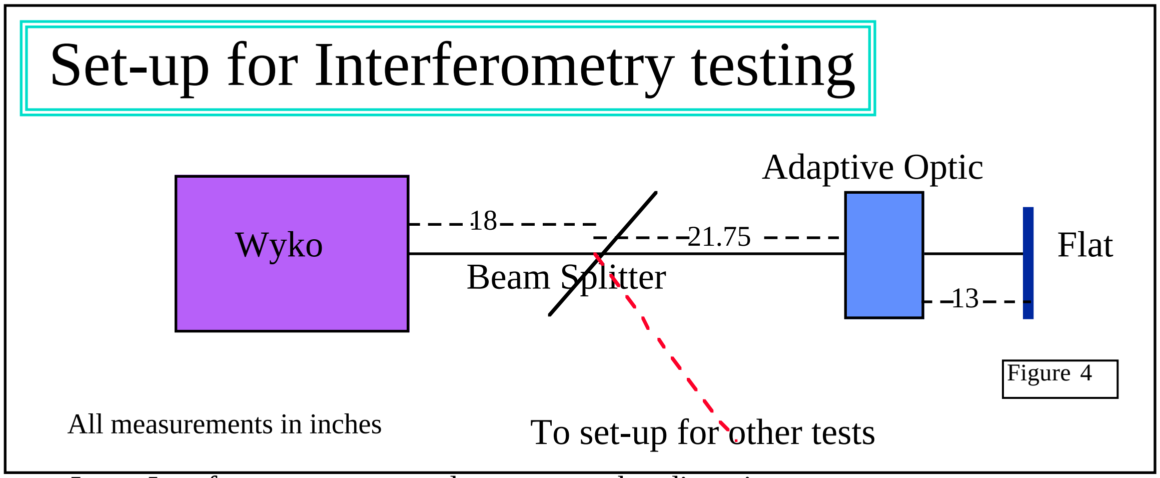

Figure 4

Laser Interferometer was used to measure that distortion.

Figure 4 is the set-up for this test. The beam travels from the Wyko through the optic to a flat. The flat reflects it back through the optic and then back into the Wyko, where the wavefront is measured. The results are displayed on a connected computer using Vision software [8]. The raw data can be exported, as was done in this case, to other programs for further analysis.

Beam Propagation

Beam Propagation is used to determine the appearance of the beam at various longitudinal locations. Three positions were used for each measurement: a re-imaged lens plane, and a forward and backward propagation approximately equivalent to 200 m in free space. The images generated by this test indicate the intensity uniformity at various positions on the beam, with the ideal being uniform.

The set-up for Beam Propagation is in Figure 5. The Wyko was used to provide the collimated laser source. After passing through the optic twice the beam hits a beam splitter which reflects some of the beam through an optical system, which includes a telescope. The end point of this system is a CCD camera, mounted on a metal rail. The various positions required for the three measurements were achieved by moving the camera along the rail. A frame grabber was used to capture the images for this test.

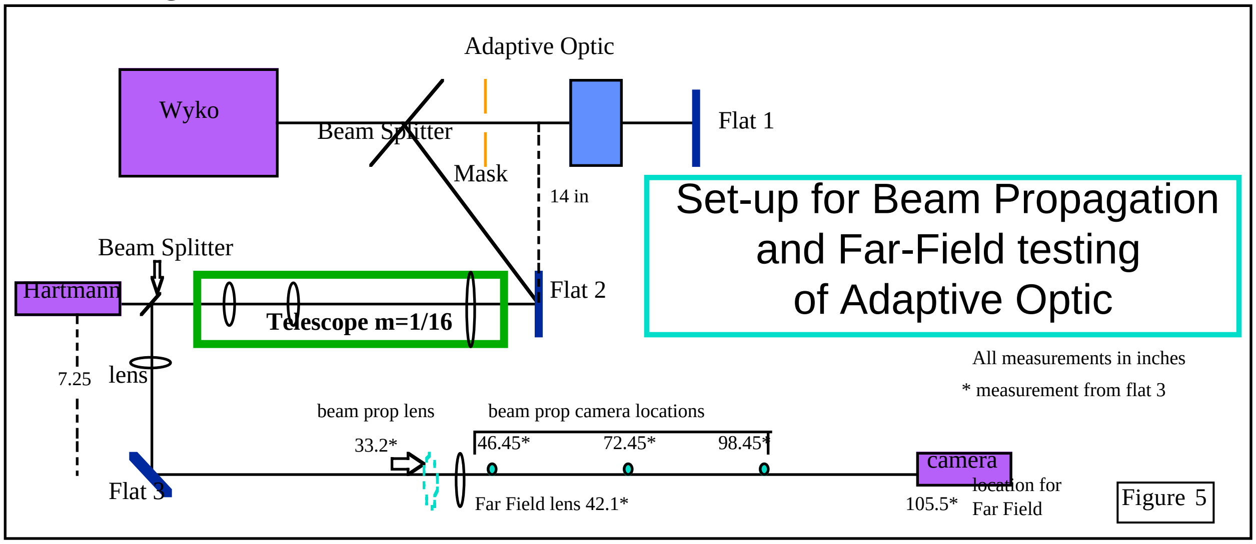

Figure 5

Far-field

The far field test measures the beam intensity profile at a propagation distance equivalent to infinity. The set-up for this test is very similar to beam propagation .The mirror indicated and the camera are moved such that the image of the beam front is focused onto the camera (Figure 5). This test is useful in determining the effects of diffraction from the optical surface. The tooling marks on Raytheon optics and the phase plate edges contribute to diffraction effects. It is important to minimize those effects. The program used to collect these images was Scion Image [9].

Presentation and Discussion of Data:

Introduction

Due to the volume of data collected, only a selection from each test is presented in this section. Some further data can be found in the appendix, including the excel worksheets used to generate the graphs of this section. Unfortunately the large number of images taken from the three tests prevents more than the sampling shown here from being included. The generalizations presented here apply to all data, shown or not.

Interferometry

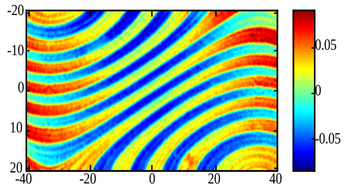

Figure 6 Interferometry image from Phase-plate part with no shear (neutral position).

The wavefront images generated by this test must be processed to obtain numerical data, but alone they still contribute to our understanding of the optics. In the ideal situation optics in their neutral position would produce an unaffected wavefront. Figure 6 is the wavefront image of the Phase-plate part in its neutral position. The lines in the image are caused by the profile of the optic. These lines will most likely cause the diffraction effects we see in later tests. The Raytheon part is not without its own imperfections. The image from its neutral position (Figure 7), while flatter than the image from the Phase-plate part, has an almost circular pattern. This pattern is most likely caused by tooling marks from fabrication. Attempts were made to minimize the tooling marks. The resulting figure is within specified tolerance.

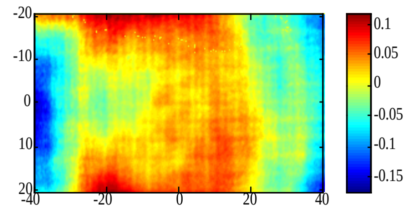

Figure 7 Interferometry image from Raytheon part with no shear (neutral position).

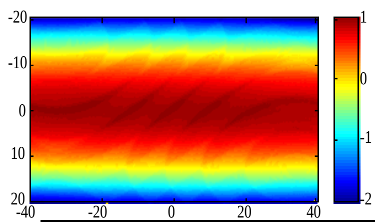

Figure 8 Interferometry Image from Phase-plate part with 10 mm shear on the x-axis.

When the optical elements are translated, the astigmatism produced is apparent in the images of the wavefront. When the elements are shifted on the x-axis a horizontal pattern is produced(Figure 8), indicating astigmatism in the x-axis, as predicted. The same holds true of shifts along the y-axis(Figure 9). In the phase-plate images (Figure X) the profile of the optics seen at no shear are still evident. These profile lines will most likely cause diffraction effects. They also blur the edges of the pattern shown and contribute to the error in the PV, RMS and sag readings. The lines themselves can be partly attributed to the wavelength of the laser used for testing. The optics were designed for a 600-nm laser and a 633-nm laser was used.

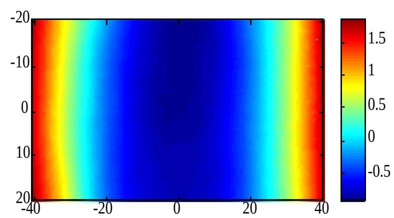

Figure 9 Interferometry Image from Raytheon part with 10 mm shear on the y-axis.

The numerical data from this test can be summarized in four graphs for each optic. Each measurement produced an image of the wavefront, from which Peak to Valley (PV) and RMS values are calculated. Using the Vision software [8] to remove Tilt, Power and Astigmatism we can find the residual data for PV and RMS. The difference between PV and sag is the residual error of the optics.

The graphs of PV and Residual RMS compare the experimental PV (at 600 nm), with the ideal based on the design specifications. The equation to determine the ideal PV or sag is: $\lambda = 0.3 \cdot S$, where λ is the number of waves and S is the shear on either axis. To calculate the ideal value for the translations off axis (shear in both x and y) calculate the waves for each axis and add them together. The experimental measurements are accurate, however, they do not show exactly was of importance(Figure 10,11,14,15). To examine this more closely a sag measurements were taken. These measurements will more accurately represent the performance of the optic. The sag measurements were performed by fitting a second order polynomial to the interferometric data. The coefficients of the fit were used to determine sag over a given beam width. This information (Figure X) confirms expectations of performance. The sag measurements for the Raytheon optic have opposite slope from those for the Phase-plate optic because of the difference in optical placement described in the Methodology section.

Another interesting development can be deduced form the PV graph for the Raytheon optic for displacement along the y-axis (Figure 11). The PV graph appears shifted to the right of the ideal. Closer examination of the vertex of the graph indicates that the zero on the y-axis is not at the center of the optic, but rather at 0.5 mm in the positive y-direction. Further readings were taken assuming the zero at this new position.

Measurements from Raytheon Optic

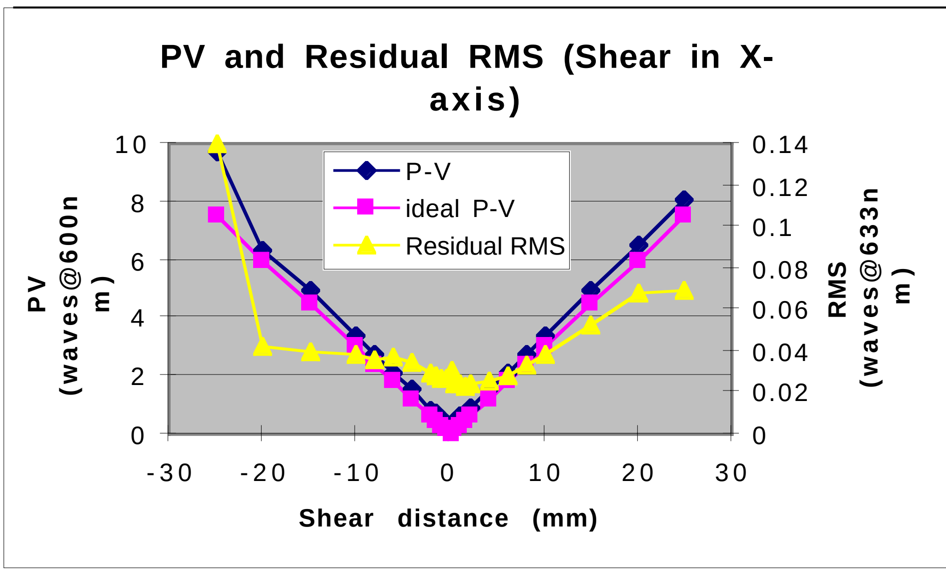

Figure 10

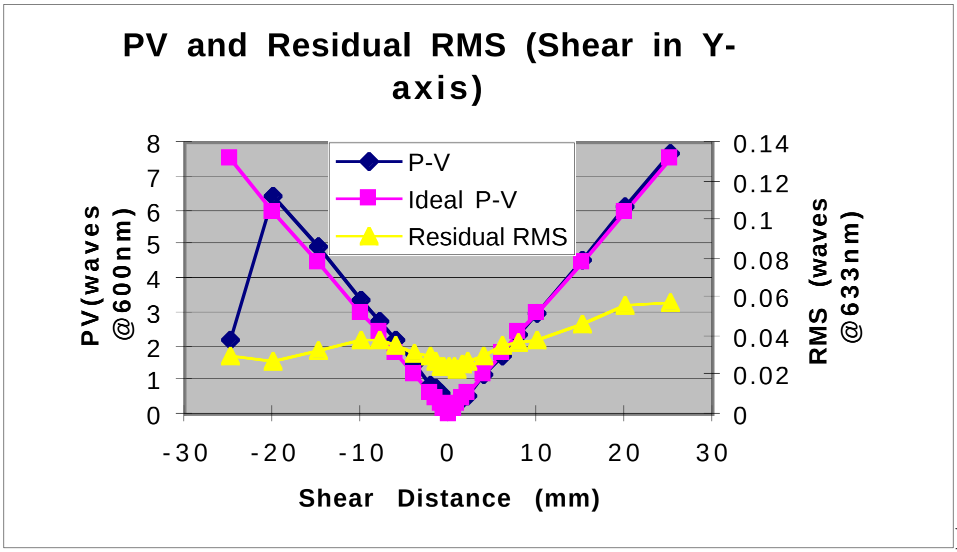

Figure 11

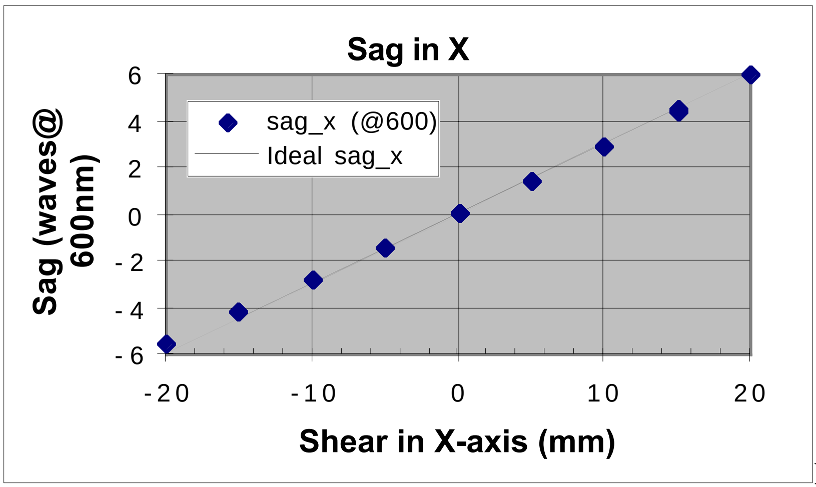

Figure 12

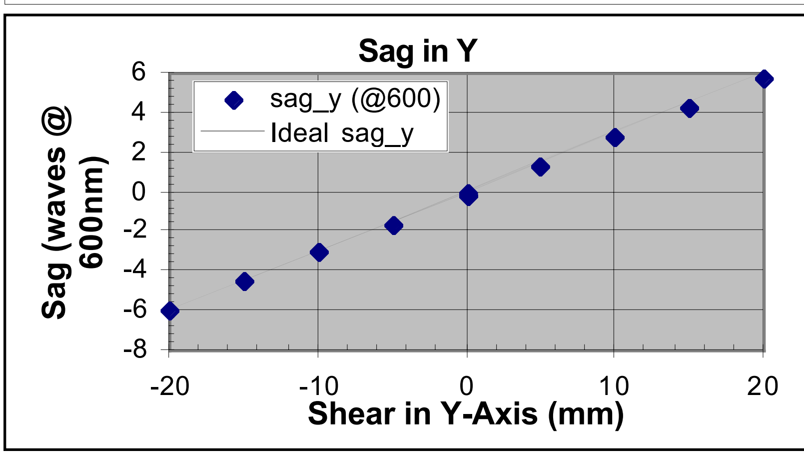

Figure 13

Measurements from 16-level Phase-Plate Optic

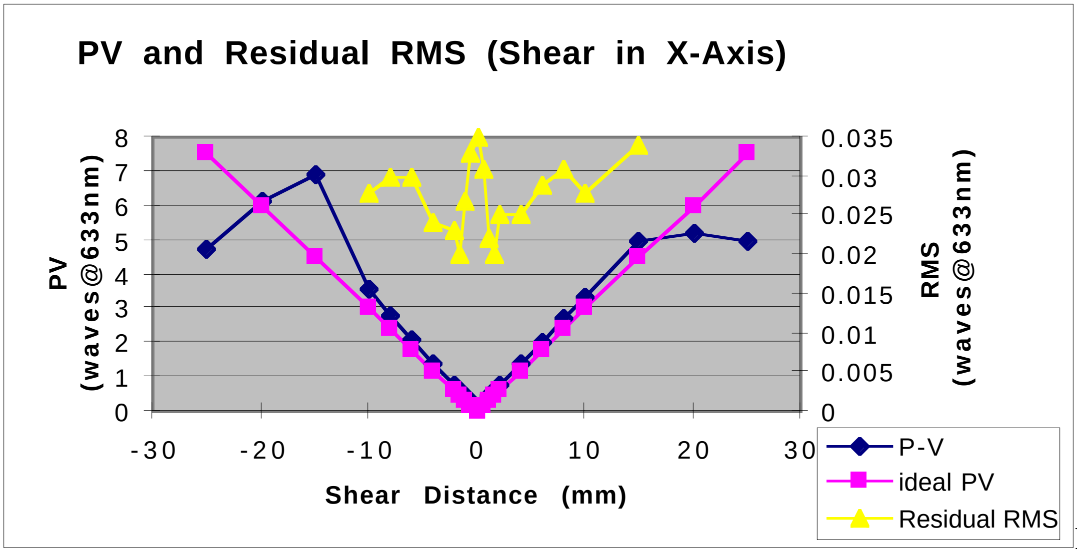

Figure 14

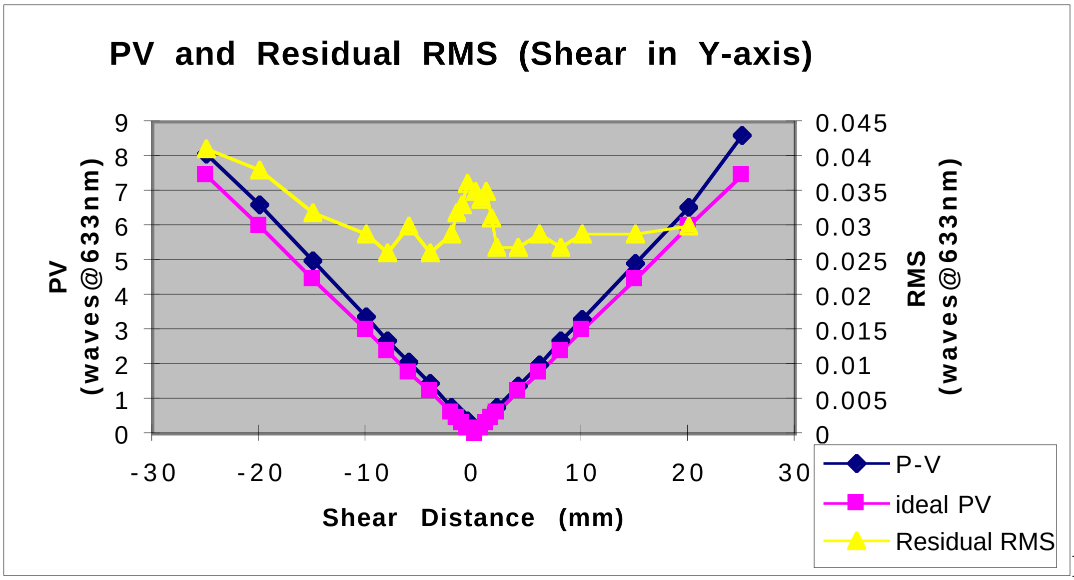

Figure 15

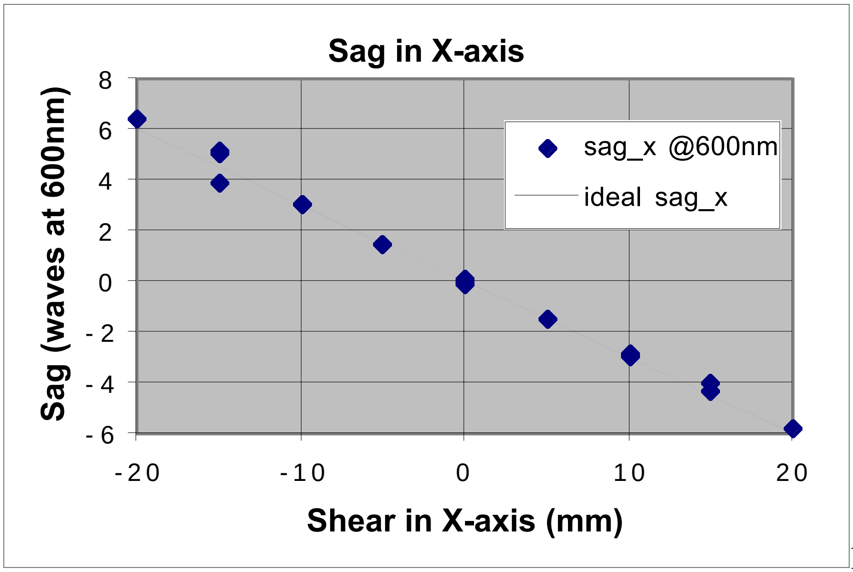

Figure 16

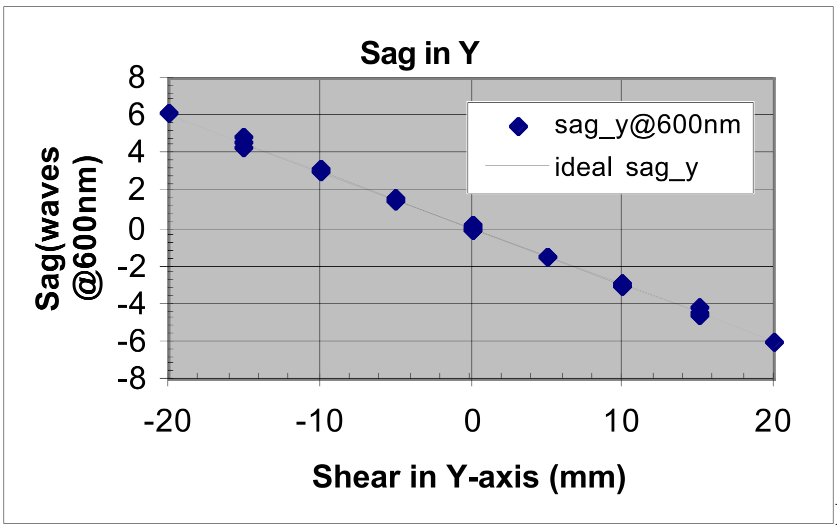

Figure 17

Because the impact of this new "zero" point did not produce significant changes when the optics are translated with relationship to each other, the interferometer data was not retaken. The new zero was used for the beam propagation test.

The data points generated with higher shear values do not appear as accurate as those closer to the neutral position. The Wyko is limited by the slope of the wavefront. When the wavefront has a high slope value the Wyko is unable to get an accurate reading. Greater shear on the optics produces more astigmatism and therefore more slope on the wavefront. These high-shear data points may be inaccurate as a result of the limitations of the Wyko rather than the optic itself. Also contributing may be the edge of the optics and the mounting devices. These would increase diffraction effects should the wavefront come in contact with them during the test. It is also possible that the quality of the optic is better at the center than at the edges. These two features would only minimally affect the readings in comparison to the limitations of the Wyko.

Beam Propagation

Beam propagation is used to test the beam intensity uniformity at several longitudinal positions relating to a relayed image of the optic. Ideally when the optic is in its neutral position the beam should have uniform intensity. The Igor program[10] was used to analyze the captured images from beam propagation. It calculated the percent of the image falling into each of two categories: greater than twice the mean intensity and less than half the mean intensity. This is a quantifiable measurement of beam uniformity. A comparison of the beam uniformity from the Raytheon optics and the Phase-plate optics is also useful. The beam was propagated through the center of each optic in the neutral position, and the four corners (still in the neutral position). Using the corresponding Wyko information a theoretical beam propagation was done for comparison with experimental data.

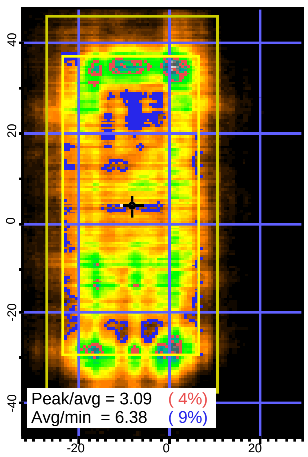

Figure 18 Experimental beam propagation of -200m through center of Raytheon optic.

General information about the optics can be deduced by examining the propagation through the center of each optic (Figure 18, 19). The corresponding theoretical propagation (Figure 20, 21) agrees well with the data collected. The Phase-plate image is much wider, and more segmented than the Raytheon image indicating diffraction effects as evidenced in the other tests. As in interferometry images, the lines of the Phase-plate are visible due to the diffraction of the beam. A more numerical examination of the intensity can be accomplished by examining the numerical data at the bottom of the image. The percentage in red (top) is the percent of the area of the beam that is greater than twice the mean intensity of the beam. The percentage in blue (bottom) is the percent of the area of the beam that is less than half the mean intensity of the beam. More generally the top number indicates the percentage of the beam much more intense, and the bottom number much less intense, than the mean intensity. A uniform beam (for example with no optic) would indicate zero percent of the beam being more intense or less intense

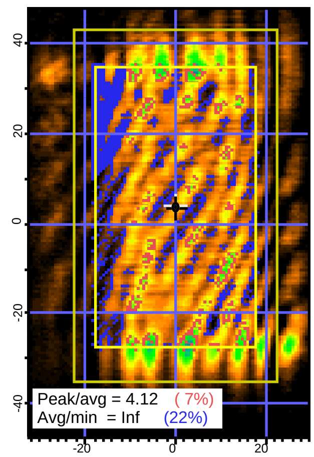

Figure 19 Experimental beam propagation of -200m through center of Phase-plate optic.

Figure 20 Theoretical beam propagation of -200 m through Raytheon optic.

Figure 21 Theoretical beam propagation of -200 m through Phase-plate optic.

than the mean. Clearly the Raytheon beam is more uniform than the Phase-plate beam. The two figures shown are at an equivalent propagation of -200 m from a relayed image of the optic, but the data collected from the other two longitudinal positions show similar information.

Another interesting feature pointed out by the beam propagation test is the quality of the corners of the optic. Figure 22 is the experimental beam propagation through the corner corresponding to a shift (in both optics) of (20 mm, -25 mm). In this position there is no optical power just a shift in the optical axis. The image appears to be skewed to one side. To further examine this feature, the theoretical beam propagation was calculated (Figure 23). The skew in the image is less obvious, but still present, revealing that further aberrations are introduced when the edges of the optic are used. The center of the optic is of higher quality than the edges. This further confirms the seemingly misplaced data points in the interferometry data graphs.

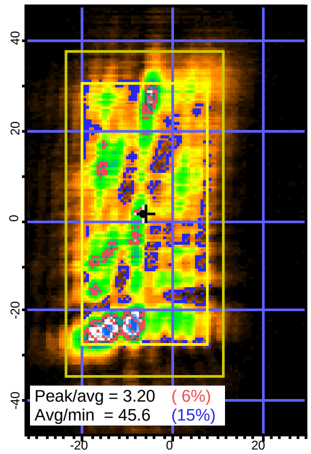

Figure 22 Experimental beam propagation of -200m through corner (20, -25) of Raytheon optic. Notice the slight skew of the image.

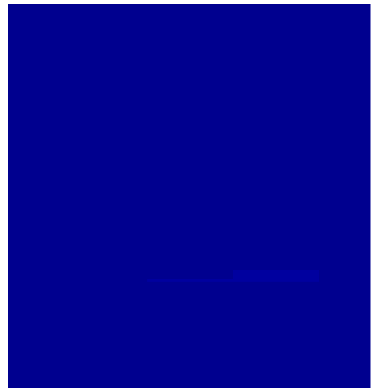

Figure 23 Theoretical beam propagation of -200 m through corner (20,-25) compare skew with figure to left.

Far Field

No numerical data has been calculated from the far-field test, however a comparison of the far-field images from the Raytheon parts and the Phase-plate parts can confirm the suggestion from the other tests that there are significant diffraction effects in the Phase-plate optics. A rectangular aperture was used in this test, meaning that if no optic is in place the system should return the diffraction pattern of a rectangular aperture (Figure 24). Ideally when the adaptive optics are in their neutral position they should not affect the diffraction pattern. Figure 25 is the Raytheon-part far-field image with the optics in the neutral position. The image is just as expected, indicating very little diffraction is occurring in the optic, only through the aperture. The phase-plate far-field image (Figure 26) shows distinct differences from the diffraction pattern of a rectangular-aperture, indicating diffraction in the optic itself. Some of the diffraction of the Phase-plate optic can be attributed to the 633 nm wavelength it was tested at, versus the design at 600 nm. Other causes of diffraction are binary mask misalignments. Far-field images through the four corners of each optic were also taken. The image of Raytheon parts is not as clean as through the center, however the difference between the Raytheon image and the corresponding phase-plate image is still significant. This again

Figure 24 A far field image with no optic in position. Diffraction pattern of a rectangular aperture.

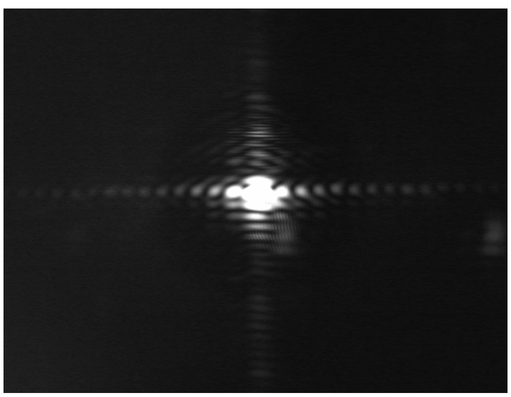

Figure 25 Far-Field image through center of Raytheon optic. Notice the rectangular aperture diffraction pattern.

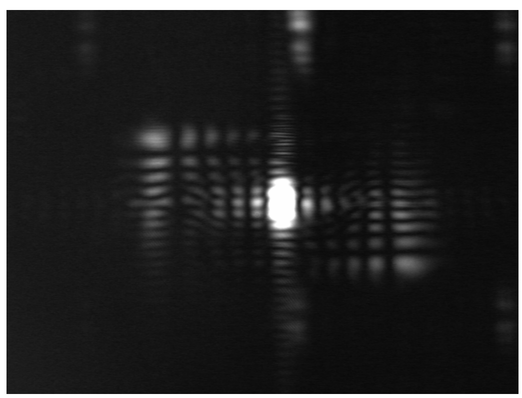

Figure 26 Far-field image through center

confirms the higher quality of the center of the optic.

Summary and Conclusion:

Two adaptive optics were characterized using interferometry, beam propagation and far field tests to determine theoretical versus experimental performance and to compare the two methods of fabrication used to produce the optics.

The optics performed as required, correcting/creating low-order astigmatic wavefronts. Tests also reveal that the center of both optics is of higher quality than the edges. The PV, RMS and sag measurements conform closely to expected values, except close to these edges.

The performance of both optics confirms the Raytheon parts were fabricated to a tighter tolerance, and therefore, the Raytheon PV, RMS and sag measurements conform more closely to expected values than the Phase-plate values. The Raytheon wavefront also had more uniform beam intensity and less diffraction, and is usable over a great band of wavelengths. Despite the better performance of the Raytheon parts, the Phase-plate optic may still be effective for some uses, at significant financial benefit, particularly in a laser system that can tolerate scatter losses.

The adaptive optical elements detailed within this report show great promise and future uses should be investigated, especially in the areas of beam processing. Using the optics in conjunction with higher-order correctors to induce larger corrections than could be achieved singly should also be considered.

References

[1] R. K. Tyson *Principles of Adaptive Optics*, Second Edition, p. 3, Academic Press, San Diego, 1998.
[2] L.W. Alvarez, 'Two-element variable-power spherical lens,' U.S. Patent #3305294 (1967).
[3] L.W. Alvarez and W. E. Humphrey, 'Variable-power lens and system,' U.S. Patent #3507565 (1970).
[4]L.W. Alvarez, 'Development of variable-focus lenses and a new refractor,' *J. Am. Optom. Assoc.* **49** (1) p. 24-29 (1978).
[5] R. K. Tyson *Principles of Adaptive Optics*, Second Edition, p. 210-219, Academic Press, San Diego, 1998.
[6] Image courtesy of Ian Barton
[7] I.M. Barton, S.N. Dixit, L.J. Summers, C.Thompson, and K.Avicola, 'A diffractive Alvarez lens, to be submitted to *Optics letters*, 1999.
[8] Wyko Vision for optical testing, Wyko Corp., version 1.800 Copyright 1996.
[9] Scion Image, an adaptation of NiH image by Wayne Rasband, National Institute of Health.
[10] Igor Pro, WaveMetrics Inc., version 3.13, copyright 1998-1998

Appendix

Interferometry data for Raytheon optic

Coordinates in table are for one element the other element would be moved just the opposite.

X Axis (mm)	Y Axis (mm)	P-V(633)	P-V (600nm)	Ideal P-V	Residual RMS
0	-25	2.116	2.23238	7.5	0.03
0	-20	6.118	6.45449	6	0.027
0	-15	4.649	4.904695	4.5	0.033
0	-10	3.181	3.355955	3	0.039
0	-8	2.607	2.750385	2.4	0.038
0	-6	2.051	2.163805	1.8	0.035
0	-4	1.443	1.522365	1.2	0.032
0	-2	0.839	0.885145	0.6	0.03
0	-1.5	0.712	0.75116	0.45	0.027
0	-1	0.561	0.591855	0.3	0.025
0	-0.5	0.429	0.452595	0.15	0.025
0	0	0.289	0.304895	0	0.025
0	0.5	0.208	0.21944	0.15	0.025
0	1	0.305	0.321775	0.3	0.024
0	1.5	0.422	0.44521	0.45	0.026
0	2	0.548	0.57814	0.6	0.027
0	4	1.092	1.15206	1.2	0.03
0	6	1.651	1.741805	1.8	0.035
0	8	2.219	2.341045	2.4	0.037
0	10	2.848	3.00464	3	0.039
0	15	4.339	4.577645	4.5	0.047
0	20	5.807	6.126385	6	0.056
0	25	7.302	7.70361	7.5	0.057
25	0	7.632	8.05176	7.5	0.07
20	0	6.208	6.54944	6	0.068
15	0	4.735	4.995425	4.5	0.053
10	0	3.194	3.36967	3	0.039
8	0	2.636	2.78098	2.4	0.033
6	0	2.023	2.134265	1.8	0.028
4	0	1.47	1.55085	1.2	0.026
2	0	0.876	0.92418	0.6	0.024
1.5	0	0.716	0.75538	0.45	0.023
1	0	0.579	0.610845	0.3	0.025
0.5	0	0.434	0.45787	0.15	0.025
0	0	0.304	0.32072	0	0.031
-0.5	0	0.352	0.37136	0.15	0.027
-1	0	0.54	0.5697	0.3	0.027
-1.5	0	0.676	0.71318	0.45	0.028
-2	0	0.826	0.87143	0.6	0.03

-4	0	1.437	1.516035	1.2	0.035
-6	0	2.028	2.13954	1.8	0.037
-8	0	2.629	2.773595	2.4	0.036
-10	0	3.225	3.402375	3	0.039
-15	0	4.672	4.92896	4.5	0.04
-20	0	6.036	6.36798	6	0.042
-25	0	9.246	9.75453	7.5	0.14
1	1	0.591	0.623505	0.6	0.025
-1	1	0.466	0.49163	0.6	0.028
-1	-1	0.78	0.8229	0.6	0.029
1	-1	0.79	0.83345	0.6	0.026
5	5	2.8	2.954	3	0.034
-5	5	2.751	2.902305	3	0.035
-5	-5	3.17	3.34435	3	0.04
5	-5	3.083	3.252565	3	0.031
10	10	5.752	6.06836	6	0.053
-10	10	5.591	5.898505	6	0.21
-10	-10	6.04	6.3722	6	0.044
10	-10	5.937	6.263535	6	0.04
15	15	8.887	9.375785	9	0.054
-15	15	8.435	8.898925	9	0.032
-15	-15	9.016	9.51188	9	0.042
15	-15	8.815	9.299825	9	0.041
Using .5 in Y as zero					
0	10	2.825	2.980375	3	0.041
0	-10	3.078	3.24729	3	0.039

Sag measurements for Raytheon Optic

x	y	sag_x	sag_y	sag_x (@600)	sag_y (@600)	Ideal sag_x	Ideal sag_y
0	0	0.039	-0.1318	0.041132	-0.139005	0	0
0	10	0.049	2.6235	0.0516787	2.766918	0	3
0	15	0.0545	3.99	0.0574793	4.20812	0	4.5
0	20	0.053	5.391	0.0558973	5.685708	0	6
5	5	1.395	1.242	1.47126	1.309896	1.5	1.5
5	-5	1.386	-1.542	1.461768	-1.626296	1.5	-1.5
-5	5	-1.315	1.252	-1.386887	1.3204427	-1.5	1.5
-5	-5	-1.318	-1.541	-1.390051	-1.625241	-1.5	-1.5
10	10	2.788	2.647	2.9404107	2.7917027	3	3
-10	10	-2.664	2.616	-2.809632	2.759008	-3	3
10	0	2.764	-0.01327	2.9150987	-0.013995	3	0
-10	0	-2.666	-0.142	-2.811741	-0.149763	-3	0
10	-10	2.773	-2.903	2.9245907	-3.061697	3	-3
15	15	4.235	4.093	4.4665133	4.3167507	4.5	4.5
-15	15	-3.957	4.005	-4.173316	4.22394	-4.5	4.5
15	0	4.2	-0.129	4.4296	-0.136052	4.5	0
-15	0	-3.985	-0.174	-4.202847	-0.183512	-4.5	0
15	-15	4.175	-4.25	4.4032333	-4.482333	4.5	-4.5
-15	-15	-3.983	-4.308	-4.200737	-4.543504	-4.5	-4.5
20	0	5.668	-0.127	5.9778507	-0.133943	6	0
-20	0	-5.291	-0.19	-5.580241	-0.200387	-6	0
0	-20	0.0407	-5.6641	0.0429249	-5.973737	0	-6
0	-15	0.0407	-4.2894	0.0429249	-4.523887	0	-4.5
0	-10	0.0369	-2.9202	0.0389172	-3.079838	0	-3

Interferometry data for Phase-plate optic

Coordinates in table are for one element the other element would be moved just the opposite. Blanks indicate the Wyko was unable to get an accurate measurement for that position.

X Axis (mm)	Y Axis (mm)	P-V (633nm)	P-V(600nm)	ideal PV	Residual RMS
0	-25	7.691	8.114005	7.5	0.041
0	-20	6.28	6.6254	6	0.038
0	-15	4.711	4.970105	4.5	0.032
0	-10	3.216	3.39288	3	0.029
0	-8	2.559	2.699745	2.4	0.026
0	-6	1.948	2.05514	1.8	0.03
0	-4	1.369	1.444295	1.2	0.026
0	-2	0.76	0.8018	0.6	0.029
0	-1.5	0.586	0.61823	0.45	0.032
0	-1	0.457	0.482135	0.3	0.033
0	-0.5	0.365	0.385075	0.15	0.036
0	0	0.148	0.15614	0	0.035
0	0.5	0.243	0.256365	0.15	0.034
0	1	0.373	0.393515	0.3	0.035
0	1.5	0.512	0.54016	0.45	0.031
0	2	0.7	0.7385	0.6	0.027
0	4	1.295	1.366225	1.2	0.027
0	6	1.86	1.9623	1.8	0.029
0	8	2.555	2.695525	2.4	0.027
0	10	3.154	3.32747	3	0.029
0	15	4.658	4.91419	4.5	0.029
0	20	6.18	6.5199	6	0.03
0	25	8.148	8.59614	7.5	
25	0	4.709	4.967995	7.5	
20	0	4.949	5.221195	6	
15	0	4.738	4.99859	4.5	0.034
10	0	3.158	3.33169	3	0.028
8	0	2.563	2.703965	2.4	0.031
6	0	1.933	2.039315	1.8	0.029
4	0	1.308	1.37994	1.2	0.025
2	0	0.731	0.771205	0.6	0.025
1.5	0	0.611	0.644605	0.45	0.02
1	0	0.405	0.427275	0.3	0.022
0.5	0	0.248	0.26164	0.15	0.031
0	0	0.172	0.18146	0	0.035
-0.5	0	0.293	0.309115	0.15	0.033
-1	0	0.412	0.43466	0.3	0.027
-1.5	0	0.587	0.619285	0.45	0.02
-2	0	0.746	0.78703	0.6	0.023

-4	0	1.357	1.431635	1.2	0.024
-6	0	1.995	2.104725	1.8	0.03
-8	0	2.646	2.79153	2.4	0.03
-10	0	3.401	3.588055	3	0.028
-15	0	6.516	6.87438	4.5	
-20	0	5.794	6.11267	6	
-25	0	4.465	4.710575	7.5	
1	1	0.621	0.655155	0.6	0.019
-1	1	0.629	0.663595	0.6	0.031
-1	-1	0.67	0.70685	0.6	0.022
1	-1	0.677	0.714235	0.6	0.028
5	5	2.963	3.125965	3	0.03
-5	5	3.03	3.19665	3	0.029
-5	-5	3.082	3.25151	3	0.029
5	-5	3.047	3.214585	3	0.029
10	10	5.934	6.26037	6	0.031
-10	10	6.01	6.34055	6	0.029
-10	-10	9.336	9.84948	6	
10	-10	5.955	6.282525	6	0.032
15	15	9.458	9.97819	9	

Sag data for Phase-plate optic

x	y	sag_x	sag_y	sag_x @600nm	sag_y @600nm	ideal sag_x	ideal sag_y
0	0	4.93E-04	0.0509	0.000520115	0.0536995	0	0
20	0	-5.4428	-0.0662	-5.742154	-0.069841	-6	0
15	15	-4.1132	-4.4212	-4.339426	-4.664366	-4.5	-4.5
15	-15	-3.766	4.1569	-3.97313	4.3855295	-4.5	4.5
15	0	-4.1155	-0.0954	-4.3418525	-0.100647	-4.5	0
10	10	-2.7344	-2.9332	-2.884792	-3.094526	-3	-3
10	-10	-2.8118	2.8466	-2.966449	3.003163	-3	3
10	0	-2.7806	-0.0649	-2.933533	-0.0684695	-3	0
5	5	-1.374	-1.4441	-1.44957	-1.5235255	-1.5	-1.5
5	-5	-1.4094	1.4541	-1.486917	1.5340755	-1.5	1.5
0	20	0.0793	-5.7181	0.0836615	-6.0325955	0	-6
0	15	0.0661	-4.2768	0.0697355	-4.512024	0	-4.5
0	10	0.0432	-2.8513	0.045576	-3.0081215	0	-3
0	-20	-0.071	5.8736	-0.074905	6.196648	0	6
0	-15	-0.0505	4.3868	-0.0532775	4.628074	0	4.5
0	-10	-0.0322	2.9472	-0.033971	3.109296	0	3
-20	0	6.1058	0.2477	6.441619	0.2613235	6	0
-15	15	3.664	-3.9215	3.86552	-4.1371825	4.5	-4.5
-15	-15	4.8758	4.6085	5.143969	4.8619675	4.5	4.5
-15	0	4.7447	0.0826	5.0056585	0.087143	4.5	0
-10	10	2.8855	-2.7668	3.0442025	-2.918974	3	-3
-5	5	1.4303	-1.3484	1.5089665	-1.422562	1.5	-1.5
-5	-5	1.3956	1.5099	1.472358	1.5929445	1.5	1.5
-10	-10	2.8686	3.0746	3.026373	3.243703	3	3
-10	0	2.8459	0.1326	3.0024245	0.139893	3	0